In Situ Scanning Tunneling Microscopy Examination of Molecular Adlayers of Haloplatinate Complexes and Electrochemically Produced Platinum Nanoparticles on Au(111)

Yoshiki Nagahara,[†] Masanori Hara,[†] Soichiro Yoshimoto,[†] Junji Inukai,[†] Shueh-Lin Yau,[‡,§] and Kingo Itaya*[,†,‡]

Department of Applied Chemistry, Graduate School of Engineering, Tohoku University, Aobayama 04, Sendai 980-8579, Japan, and CREST, JST, 4−1−8 Kawaguchi, Saitama 332-0012, Japan

Received: September 2, 2003; In Final Form: December 16, 2003

Immersion of an ordered Au(111) electrode in a 5 ∼ 50 μM haloplatinate solution for 1 min results in spontaneous and irreversible adsorption of a submonolayer to a monolayer Pt complex. In situ STM imaging reveals the formation of highly ordered molecular adlayers of Au(111) − $(\sqrt{7} \times \sqrt{7})R19.1°$ − $PtCl_4^{2-}$ and $PtBr_4^{2-}$ ($\theta = 0.143$) in a solution containing 50 μM of each complex. Dosing in a dilute $PtBr_4^{2-}$ solution (5 μM) produces another highly ordered structure, identified as Au(111) − $(2\sqrt{19} \times 2\sqrt{19})R23°$ − 7 $PtBr_4^{2-}$ + 6 Br. Atomic resolution STM reveals pinwheel features of the planar PtX_4^{2-} adsorbates (X = Cl, Br, I). The molecular adlayers of PtI_6^{2-} are always disordered, irrespective of the dosing conditions. The reduction potentials of these molecular overlayers to produce the deposit of metallic Pt decrease in the order of $PtCl_4^{2-}$ > $PtBr_4^{2-}$ > PtI_6^{2-}. The Pt deposit exists in the form of nanoparticles with an average diameter of 3.0 nm and height of 0.46 nm, and they are uniformly distributed on the Au(111) substrate. The electrocatalysis toward the oxygen reduction of Pt particles on Au(111) is examined with a hanging-meniscus rotating disk technique. The Pt particles prepared with the precursors of chloro- and bromoplatinate are active in catalyzing oxygen reduction, whereas those from iodoplatinate are inert. This result correlates with the strength of surface bond between halide and Au or Pt metal. Iodine adatoms evidently block the active sites on Pt clusters.

Introduction

The tantalizing properties exhibited by nanomaterials have attracted worldwide research interests. In addition to the high surface-to-volume ratio, the apparent virtue in catalysis, dubbed as "quantum effect", manifests itself by producing chemical and physical properties that are different from those of the bulk.[1] For example, while bulk metallic gold is essentially inert toward the oxidation of carbon monoxide, TiO_2^- supported gold nanoparticles with diameters of 2.0 nm readily convert CO to CO_2 at a temperature as low as 0 °C.[2] Although nanoparticles of gold have received the most attention thus far, the studies performed in electrochemical environments have mostly focused on quantized electron transfer or double-layer charging.[3]

In terms of electrocatalysis, which has important ramifications in the development of future energy resources, nanoparticles of platinum are apparently more relevant. Research in the past decade has made substantial progress in the preparation, characterization, and electrocatalysis of Pt clusters. Reduction of Pt(II) or Pt(IV) salts in aqueous solutions in the presence of appropriate capping reagents is one of the methods used to tailor the size and atomic arrangement of the Pt clusters. Alternatively, the deposition into confined spaces in materials such as zeolites, silicates, and carbon nanotubes is used to construct patterned Pt arrays.[4−9] Also, electrocatalytically inert substrates such as highly oriented pyrolytic graphite (HOPG) and polycrystalline Au are used to support Pt clusters to explore their activities toward some electrochemical reactions, including the electroxidation of CO, methanol, and formic acid molecules, the hydrogen evolution, and the reduction of oxygen molecules.[10−16] The "size effect" has been observed in most systems. For example, the oxidation of CO molecules at Pt nanoparticles with diameters less than 3.0 nm occurs at a potential ca. 100 mV more positive than that observed at polycrystalline Pt. On the other hand, smaller Pt clusters were noted to have a higher activity toward the oxygen reduction. This phenomenon is presumed to arise from the higher density of active sites on the clusters than on the bulk Pt.[10,13]

Meanwhile, researchers have used well-defined gold substrates to support electrochemically produced Pt and Pd particles, and scanning tunneling microscopy (STM) has been intensively used to characterize the size and distribution of these nanoculsters.[17−20] Uosaki et al. reported on the layer-by-layer growth of Pt atoms on atomically smooth Au(111) during the electrochemical reduction of $PtCl_6^{2-}$ complex.[17] Wabiel et al. performed a similar study and showed that Pt adatoms preferentially cluster into nanoparticles with a diameter of 10−20 nm and a height of 0.6−1.0 nm.[20] The shape of the Pt particles can be triangular, square, or random.[20] The formation of clusters, rather than layered deposits, is anticipated, as Pt is known to possess a much higher surface energy than Au.[21] Alternatively, Brankovic et al. illustrated that a pre-deposited Cu adlayer can be used as a template to control the growth of a submonolayer of Pt on a Au(111) surface.[22]

The aim of this study is to examine the structures of molecular adlayers of haloplatinates on Au(111) and to characterize the formation of reduced Pt metals by using in situ STM. As halide

* Corresponding author. E-mail:itaya@atom.che.tohoku.ac.jp; TEL: 81-22-2145380; FAX: 81-22-2145380.
† Tohoku University.
‡ CREST.
§ Department of Chemistry, National Central University, Chungli, Taiwan 320.

10.1021/jp036605+ CCC: $27.50
Published on Web 02/13/2004

anions frequently coexist with platinate complexes in solutions, they are adsorbed on the Au substrate as well as the Pt deposit, affecting not only the structure of molecular adlayers but also the activity of the as-prepared Pt particles. In particular, the Pt-modified Au(111) electrode exhibits activity toward oxygen reduction, but the electrode derived from PtI_6^{2-} is more inert than the electrodes prepared from other haloplatinate complexes, because the active sites on Pt are blocked by adsorbed iodide anions but not by other halide ions.

Experimental Section

The Au(111) single-crystal electrodes used for electrochemical experiments including voltammetric and rotating disk electrode measurements and for STM experiments were prepared by the Clavilier method.[23] The electrochemical STM cell was equipped with a Pt quasi-reference electrode and a Au counter electrode. After being annealed and quenched in Millipore water (18.3 MΩ resistivity), the Au(111) electrode was transferred into a solution containing a haloplatinate complex. Typically, the dosing solution contained a 50 μM Pt complex and the immersion time was 1 min. These conditions were effective to produce a full monolayer of Pt complexes, as indicated by STM (vide infra). The as-prepared Au(111) electrode was first rinsed with ultrapure water after it was emersed from the dosing solution, followed by transferring through air into an STM cell. A 0.1 M $HClO_4$ solution was added to bring the system under potential control. The potential of Au(111) was always set at the open-circuit potential, ca. 0.95 V, to initiate STM imaging experiments.

All haloplatinate complexes (K_2PtCl_4, K_2PtBr_4, and K_2PtI_6) in ultrapure grade were purchased from Aldrich Chemicals (St. Louis, MO) and $HClO_4$ was obtained from Kanto Chemicals (Tokyo, Japan). They were used without further purification. All electrochemical and STM experiments were carried out in 0.1 M $HClO_4$ prepared with Millipore water.

It is difficult to remove the platinum deposit on Au(111) by electrochemical methods. However, because the amount of Pt produced by the electrochemical reduction in this study was less than a monolayer, an extensive potential cycling between 0 and 2.0 V in 0.1 M HCl allowed complete dissolution of the Pt deposit. This procedure inevitably roughened the Au(111) surface, but prolonged annealing with a hydrogen torch could restore the original surface.

The STM used was a Nanoscope E (Digital Instruments, Santa Barbara, CA) with a high-resolution scanner (maximum scan size ca. 500 nm). The tip was made of a Pt/Ir wire (diameter 0.25 mm) etched with 20 V AC in a $CaCl_2$/HCl solution. The tip was further insulated with transparent nail polish to block the faradic current. The constant-current imaging mode was used throughout this study. The STM cell was equipped with a Pt quasi-reference electrode and a Au counter electrode.

The voltammetric and rotating disk electrode experiments were performed in the three-electrode configuration, equipped with a Pt wire as the counter electrode and a reversible hydrogen reference electrode (RHE). In all electrochemical measurements, the contact of Au(111) to the electrolyte was made by submerging the bead entirely in the electrolyte first and then slowly pulling it upward to render hanging meniscus of the (111) plane. The potential scan rate was typically 50 mV/s. The study of the activity of particulate Pt on Au(111) toward oxygen reduction was conducted in 0.1 M $HClO_4$ saturated with ultrapure O_2.

Results and Discussion

Linear Sweep Voltammetry. Figure 1a shows cyclic voltammograms recorded at 50 mV/s with a Au(111) electrode coated with a monolayer of $PtCl_4^{2-}$ in 0.1 M $HClO_4$. The potential was first swept negatively from the open-circuit potential (OCP) of approximately 0.95 V. Only one reduction peak is seen at 0.73 V, followed by a mostly featureless $i-E$ profile before the precipitous increase of current at 0.05 V. The reduction peak at 0.73 V appeared only in the first negative-going potential scan, and the subsequent scans were featureless in this potential range, as shown by the dotted line in Figure 1a. Thus, this peak is believed to have resulted from the reduction of surface-bound $PtCl_4^{2-}$ molecules to Pt(0), which deposited on the Au(111) electrode. The peak potential is close to the calculated value of 0.579 V (vs Ag/AgCl) for this reaction.[24]

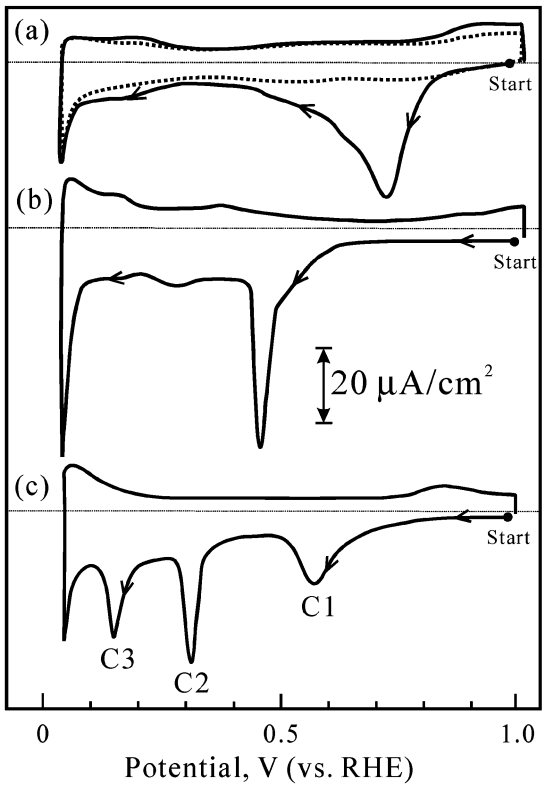

Figure 1. Cyclic voltammograms at 50 mV/s for Au(111) coated with molecular adlayers of $PtCl_4^{2-}$ (a), $PtBr_4^{2-}$ (b), and PtI_6^{2-} (c) in 0.1 M $HClO_4$. The solid and dotted traces in (a) represent the first and second potential sweeps, respectively.

Once Pt adatoms cover the entire surface of Au(111), interfacial redox reactions of hydrogen adsorption/desorption and hydrogen evolution should proceed at those potentials observed with the polycrystalline Pt electrode. The former process resulted in the minor increase of current observed between 0.35 and 0.05 V. Also, the $i-E$ profile between 0.5 and 1.0 V in the 2nd scan was featureless (dotted line in Figure 1a), suggesting that the oxide formation and reduction at Pt clusters commenced at more positive potentials than those at polycrystalline Pt. Pt nanoparticles deposited on HOPG exhibit similar properties when the size is less than 4.0 nm.[11] The in situ STM results of the present study (vide infra) indicate that most Pt particles are indeed smaller than 4.0 nm.

These results clearly show the formation of a stable monolayer of $PtCl_4^{2-}$ on Au(111), which survived the immersion in 0.1 M $HClO_4$. In contrast, the molecular adlayer of $PtCl_6^{2-}$ was not stable to the process of emersion, as it was found to be removed upon rinsing with aqueous solutions.[17] Thus, $PtCl_4^{2-}$ appears to be more strongly adsorbed on Au(111) than is $PtCl_6^{2-}$. The reduction peak at 0.73 V contains roughly 60 μC/cm^2, not

including the double-layer charging current in this potential range. The coverage of $PtCl_4^{2-}$ on Au(111) is calculated to be 0.14, assuming a $2e^-$ reduction process of Pt(II) to Pt(0). On the other hand, a previous study of $PtCl_4^{2-}$ at Au(111) in sulfuric acid indicates that the reduction process is sluggish,[20] despite the fact that, as shown by in situ STM, the adsorbed monolayer of $PtCl_4^{2-}$ is highly ordered. We can only conjecture that the supporting electrolyte may play a role in this reaction. For example, the sulfate anions in the medium used in the previous study might coordinate with the Pt(II) centers in the $PtCl_4^{2-}$ complex, possibly stabilizing the complex substantially to make it more difficult to be reduced.

To study the effect of ligands on the reduction of haloplatinate complexes, we examined two other Pt complexes, $PtBr_4^{2-}$ and PtI_6^{2-}, which were reduced in a manner similar to that used for the reduction of $PtCl_4^{2-}$. The cyclic voltammograms of these Pt complexes are shown in Figure 1b and c. The result obtained with $PtBr_4^{2-}$ is self-explanatory. The peak at 0.45 V is attributed to the reduction of surface-bound $PtBr_4^{2-}$. This reduction current, however, commences at 300 mV more negative than that of $PtCl_4^{2-}$. It is much sharper; the full width at half-maximum (fwhm) is only 20 mV, as compared to 180 mV for $PtCl_4^{2-}$ at the scan rate of 50 mV/s. This reduction peak was seen only in the first negative-going potential sweep, indicating that the entire $PtBr_4^{2-}$ monolayer is reduced during a single potential sweep. In other words, the reduction of $PtBr_4^{2-}$ is kinetically fast. The amount of charge contained in this feature is approximately the same as that of $PtCl_4^{2-}$, suggesting that these two complexes might have similar packing densities and structures on Au(111).

The *i-E* profile for PtI_6^{2-} is expectedly more complicated, as the Pt metal center possesses a higher valence of 4. Indeed, the voltammogram in Figure 1c shows three distinct peaks at 0.56 (C1), 0.32 (C2), and 0.15 V (C3), prior to the hydrogen evolution at 0.05 V. The former two peaks are associated with the stepwise reduction of Pt(IV) to Pt(II), then to Pt(0) while the third peak is due to the reduction of iodine adatoms to iodide at the Au electrode. The first two features are sharp (fwhm = 50 mV/s) and they are seen only in the first negative-going potential scan, indicating that they are kinetically facile. However, the current density for C2 ($Pt^{4+/2+}$) is lower by 30−50% than the corresponding values observed with $PtCl_4^{2-}$ and $PtBr^{2-}$, implying a lower surface coverage for PtI_6^{2-}. Since all monolayers were prepared similarly, the lower coverage could stem from the fact that PtI_6^{2-} complexes compete with other adsorbates such as free iodide anions for surface sites. This view is confirmed by the in situ STM results described.

In Situ STM Imaging of Haloplatinate Adlayers on Au(111). *Tetrachloroplatinate Complex.* The adsorption of $PtCl_4^{2-}$ on Au(111) was previously examined by in situ STM, and details of this system can be found elsewhere.[20] Our present in situ STM imaging revealed a Au(111) − $(\sqrt{7} \times \sqrt{7})R19.1$ − $PtCl_4^{2-}$ ($\theta = 0.14$) structure at 0.9 V, as shown in Figure 2a and b. This structure has two rotational domains marked as **I** and **II** in Figure 2a. Furthermore, the high resolution STM image in Figure 2b, obtained with 3 mV bias voltage and 4 nA feedback current, reveals each molecule as a centered square. This result is readily explained by the square planar molecular shape of $PtCl_4^{2-}$ where five spots, consisting of a Pt^{2+} cation at the center and four Cl^- anions at four corners of a square. The former appears to be 0.06 nm higher than the latter. Generally, imaging conditions (I_{tip}, V_b, and sharpness of the tip) and registries of admolecules determine the appearance of admolecules in STM molecular resolution. The molecular

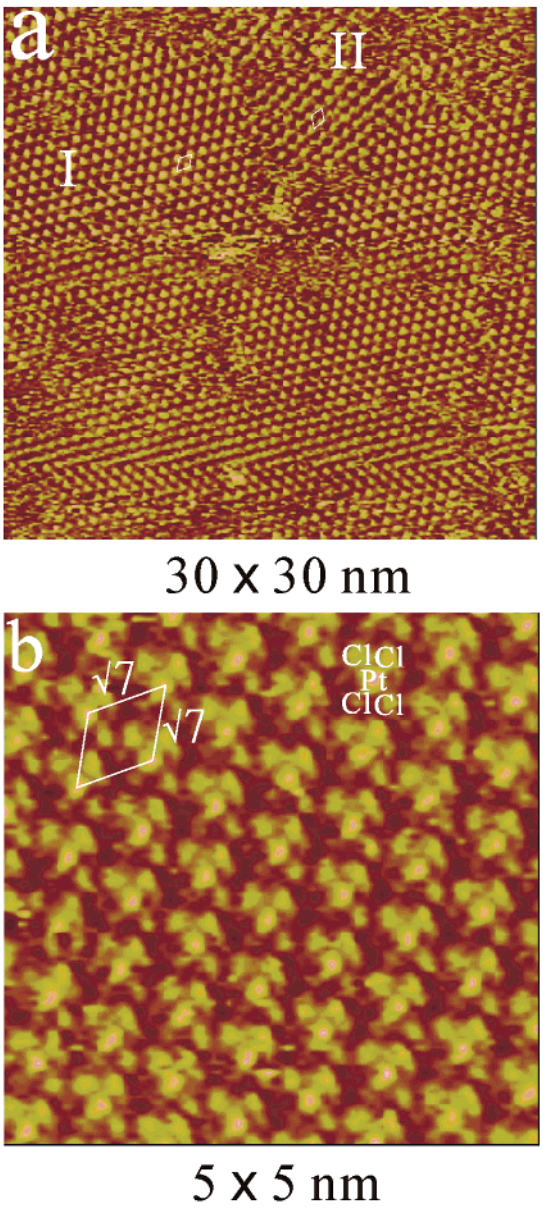

Figure 2. In situ STM image showing the structure of Au(111) − $(\sqrt{7} \times \sqrt{7})R19.1°$ − $PtCl_4^{2-}$ monolayer formed by immersion in a 50 μM K_2PtCl_4 solution. The supporting electrolyte is 0.1 M $HClO_4$ and the potential of Au(111) is 0.9 V. I_{tip} and V_b are 2−5 nA and 4−15 mV, respectively.

resolution achieved by us appears to be superior to that reported by others for $PtCl_4^{2-}$ and $PtCl_6^{2-}$ chemisorbed on Au(111).[18,20]

Tetrabromoplatinate Complex. Evidently, experimental conditions such as [PtX_4^{2-}] and immersion time dominate the coverage and structure of the adlayer. In this study the dosing time was fixed at 1 min to examine the effect of concentration on the real-space structure of $PtBr_4^{2-}$. It was found that concentrations higher than 50 μM yielded the same real-space structures. STM results obtained with 5 and 50 μM $PtBr_4^{2-}$ are illustrated. The imaging parameters of low tunneling current (1∼2 nA) and high bias voltage (100∼200 mV) revealed clear topography features of Au(111) consisting of typical characteristics of single crystalline electrodes. Atomically flat terraces frequently span a distance of more than 100 nm and they are terminated by sharp monatomic steps ($\Delta z = 2.4$ Å). The Au(111) surface is expected to be unreconstructed at 0.95 V and contained islands with a monatomic height.[19] However, the halide anions in the dosing solution could facilitate electro-

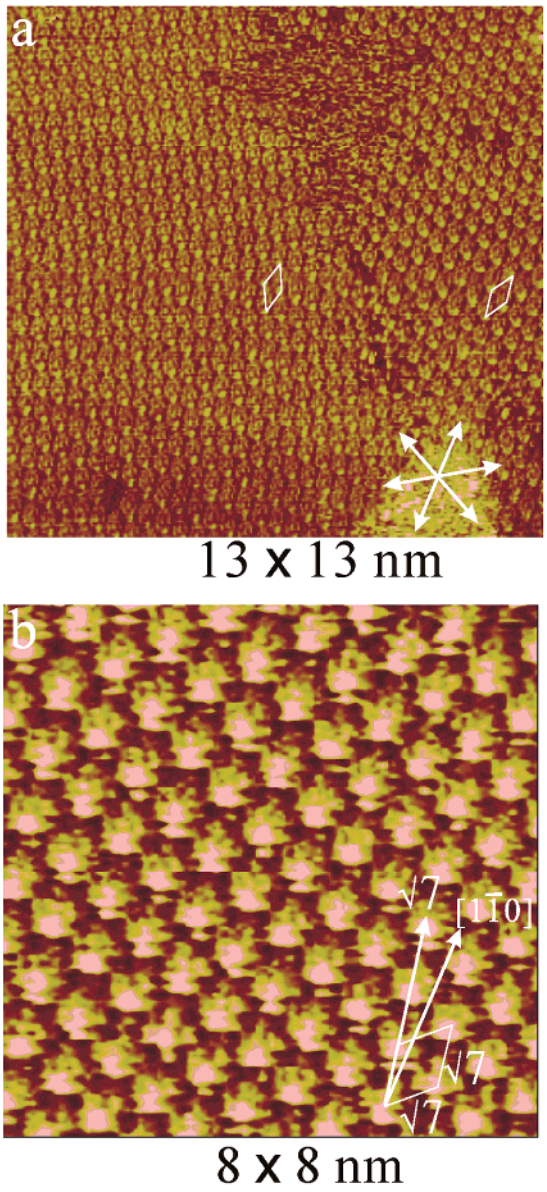

Figure 3. In situ STM images showing the domain boundary (a) and molecular resolution in Au(111) − ($\sqrt{7} \times \sqrt{7}$)*R*19.1° − $PtBr_4^{2-}$ formed by immersion in a 50 μM K_2PtBr_4 solution. I_{tip} and V_b are 2−5 nA and 15−20 mV, respectively.

chemical annealing to remove islands produced in the process of reconstruction lifting.[19] Nucleation of multiple layers of Pt complexes are sometimes observed at surface defects such as steps and pits to produce protruded islands. Also, increasing the immersion time could produce islands on the uniform monolayer, tentatively attributed to the growth of multilayers of Pt complexes. Eventually, it seems feasible to tune the experimental conditions to control the amounts of Pt complexes and Pt particles on the Au electrode.

The high-resolution scan (13 × 13 nm) shown in Figure 3a reveals the real-space arrangement of $PtBr_4^{2-}$ complex on Au(111). The adlayer consists of highly ordered hexagonal arrays with a nearest neighbor spacing of 0.76 Å. Because the close-packed molecular rows are rotated by 19° from the atomic rows of Au(111), which was observed with the high-resolution STM scan in the absence of adsorbates. Two arrows drawn in Figure 3b highlight the directions of a $\sqrt{7}$ unit vector and a Au(111) atomic row (marked [1$\bar{1}$0]). This adlayer is thus characterized as Au(111) − ($\sqrt{7} \times \sqrt{7}$)*R*19.1−1$PtBr_4^{2-}$, $\theta = 1/7 = 0.14$. Its two rotational domains are seen in the STM image in Figure 3a. The coverage determined from this STM molecular image agrees with that from pertinent voltammetric measurements (Figure 1b). Thus, the immersion of Au(111) electrode in 50 μM K_2PtBr_4 for 1 min was able to produce a well-ordered monolayer of $PtBr_4^{2-}$ complex. Figure 3b displays a close-up view of the domain on the left of the STM image in Figure 3a. I_{tip} and V_b for acquiring Figure 3b were 20 mV and 2 nA, respectively. Tetrabromoplatinate molecules appear as single protrusions, and their corrugation height is 0.8 ± 0.2 Å, depending on the condition of the tip and the parameters of STM imaging, as described previously.

The molecular adlayers prepared with more dilute (5 μM) K_2PtBr_4 solution will be described below. The dosing time was still 1 min. Figure 4a shows an image of a 50 × 50 nm^2 scan area of as-prepared Au(111) potentiostated at 0.9 V in 0.1 M $HClO_4$. The bias voltage and feedback current were 30 mV and 10 nA, respectively. Apparently, $PtBr_4^{2-}$ molecules are adsorbed in two different real-space arrays with the minor structure forming island-like patches in a predominantly molecular network. Measurements of intermolecular spacing and directions of close-packed molecular rows on the minor structure in the islands render an identification of the aforementioned ($\sqrt{7} \times \sqrt{7}$)*R*19.1 − $PtBr_4^{2-}$ structure. Figure 4b displays a further close-up view of the predominant structure with its unit cell outlined as the rhombus. This molecular adlayer is identified as Au(111) − ($2\sqrt{19} \times 2\sqrt{19}$)*R*23° − 7$PtBr_4^{2-}$. The unit vectors are ca. 2.6 nm long and rotated by 23° with respect to the atomic rows of Au(111). Two arrows drawn in Figure 4b point the directions of a $\sqrt{19}$ unit vector and the [1$\bar{1}$0] direction of the Au(111) substrate. Assuming that each spot corresponds to a $PtBr_4^{2-}$ molecule, its coverage is calculated to be 7/76 or 0.092, which is 36% less than that of ($\sqrt{7} \times \sqrt{7}$)*R*19.1° formed at higher dosages. This structure appears to consist of groups of 7 $PtBr_4^{2-}$, arranged in the form of a centered hexagon. Two neighboring complexes are 0.84 Å apart within a group, and two neighboring hexagons are connected in a point-to-point fashion.

The close-up view of this structure shown in Figure 4c reveals the internal molecular features of $PtBr_4^{2-}$. It is now clear that the six Pt complexes situated of the perimeters of hexagons all appear as pinwheels, while those in within the hexagon are seen as single protrusions. The central protrusion of the pinwheel feature can be assigned to a Pt^{2+} cation, appearing 0.02 nm higher than the bromide ligands located at the four corners of the pinwheels. In addition, two groups of dots, each arranged in equilateral triangles, are found inside the unit cell. The lateral length of the triangle is 0.40 nm, a reasonable value for Br atom, and it exhibits a corrugation height similar to that of Br^- anions in the Pt complex. These triangles are most likely the images of coadsorbing bromide ions or bromine atoms, with a packing density of 6/76 or 0.079. They might be attributable to impurities in the chemicals used or derived from the dissociation of $PtBr_4^{2-}$. This phenomenon of coadsorption also occurred for the more compact ($\sqrt{7} \times \sqrt{7}$)*R*19.1° but only at domain boundaries. Close examination of the high-resolution STM image in Figure 4c reveals that the six Pt complexes can have three different orientations, rotated by 120° sequentially around the hexagon. The two spots on the diagonal of a pinwheel feature are 5.6 Å apart from each other, which fits the ideal values calculated from the ionic radius of Pt^{2+} (0.80 Å) and Br^- (1.96 Å).[27]

Hexaiodoplatinate Complex. Figure 5a presents an in situ STM image of Au(111) coated with a monolayer of PtI_6^{2-} at

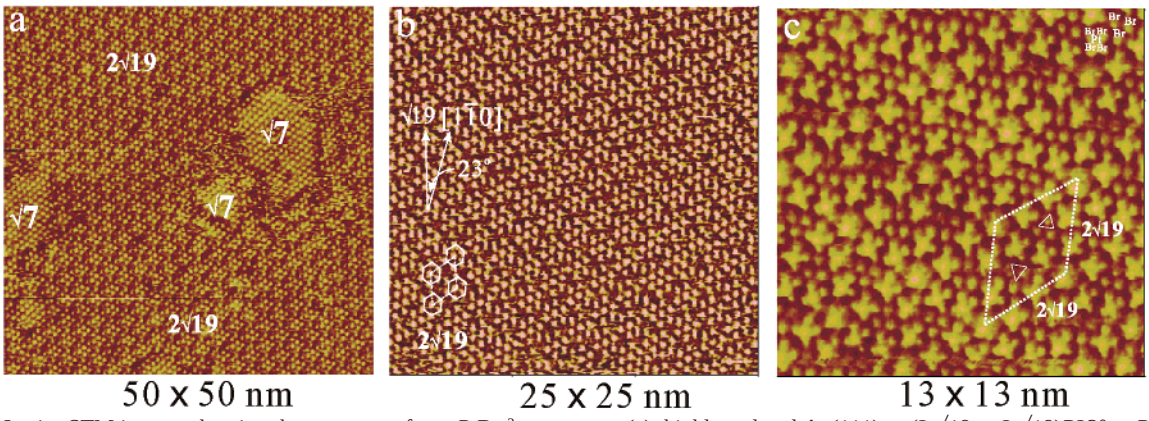

Figure 4. In situ STM images showing the presence of two $PtBr_4^{2-}$ structures (a), highly ordered Au(111) − $(2\sqrt{19} \times 2\sqrt{19})R23°$ − $PtBr_4^{2-}$ (b), and internal molecular features (c) of $PtBr_4^{2-}$. The Au(111) sample was prepared by immersion in a 5 μM K_2PtBr_4 solution for 1 min. I_{tip} and V_b are 2−10 nA and 20−30 mV, respectively.

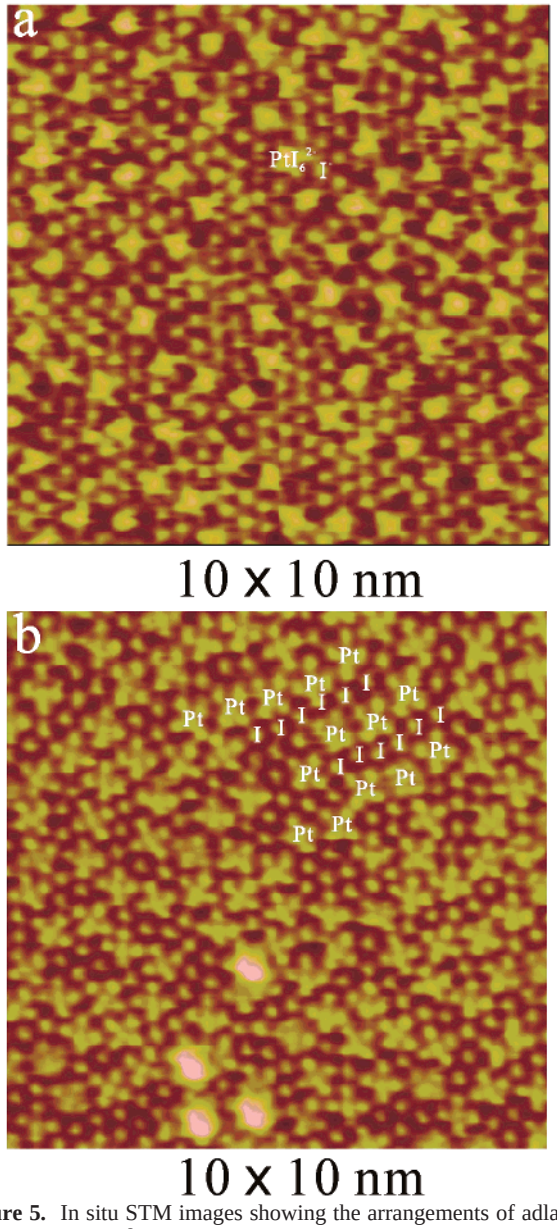

Figure 5. In situ STM images showing the arrangements of adlayers consisting of PtI_6^{2-} and I^- at 0.9 V (a) and 0.5 V (b). Sample preparation: 1 min immersion in 50 μM K_2PtI_6 solution. I_{tip} and V_b are 3−25 nA and 5−60 mV, respectively.

0.9 V. The tunneling current and the bias voltage were 3 nA and 60 mV, respectively. The concentration of K_2PtI_6 was 5 μM, and the dipping time was also 1 min. This STM image shows that the molecular adlayer lacks an order, and that there are two types of protruded features. The brighter and the dimmer features with the difference of 0.08 nm corrugation height are believed to be due to PtI_6^{2-} complexes and iodine adatoms, respectively. Thus, similarly to the case of bromoplatinate in the Au(111) − $(2\sqrt{19} \times 2\sqrt{19})R23°$ structure, free iodide ions are coadsorbed with the PtI_6^{2-} complex. However, this phenomenon of coadsorption varies with the kind of halide ions, because they interact with metals differently. Also, electrochemical potential can influence the adsorbate−substrate interaction and hence the composition and structure of the adlayers.[25,26]

Figure 5b shows an STM atomic image obtained for a PtI_6^{2-} adlayer 30 min after the potential was stepped from 0.9 to 0.5 V. The imaging parameters were 25 nA and 5 mV in this case. This STM image also reveals two types of protrusions. While the singular dots (i.e., iodine adatoms) are still present, the higher protrusions associated with PtI_6^{2-} are mostly replaced by pinwheel features attributed to the PtI_4^{2-} molecules. These pinwheel features tend to form strands lying randomly on the surface, and frequently rows of iodine adatoms and those of PtI_4^{2-} run alternatively. The distance between two iodide ligands along the diagonal of the pinwheel was 0.60 nm on the average, which agrees with the value calculated from the ionic radii of Pt^{2+} (0.08 Å) and I^- (0.22 Å).[27] These observations are in harmony with the fact that a reduction peak is seen at 0.58 V in the first negative-going potential sweep (Figure 1c), corresponding to the reduction of PtI_6^{2-} to PtI_4^{2-}.

In Situ STM Imaging of Pt Particles on Au(111). The structures of all adlayers were found to be stable toward the modulation of potential unless it was made negative enough to induce the reduction of Pt(II) or Pt(IV) to the metallic state. To observe the reduction reaction in real time, the potential of $PtBr_4^{2-}$-coated Au(111) was stepped from 0.9 to 0.4 V in the middle of a downward STM scan (Figure 6a). This perturbation of potential results in an instantaneous change in surface morphology, which is attributable to the facile reduction of Pt(II) to metallic Pt on Au(111). The surface state at 10 min after the potential step is shown in the STM image of Figure 6b, revealing evenly distributed Pt particles. The step defects located near the left edge of the STM image do not seem to cause accumulation of more Pt particles than on the terrace. The diameter of Pt particles varied between 2 and 10 nm, and they were mono- or diatomic in height. These results contrast markedly with those of the reduction of $PtCl_6^{2-}$ to Pt clusters, where step defects of Au(111) are strongly preferred.[20] However,

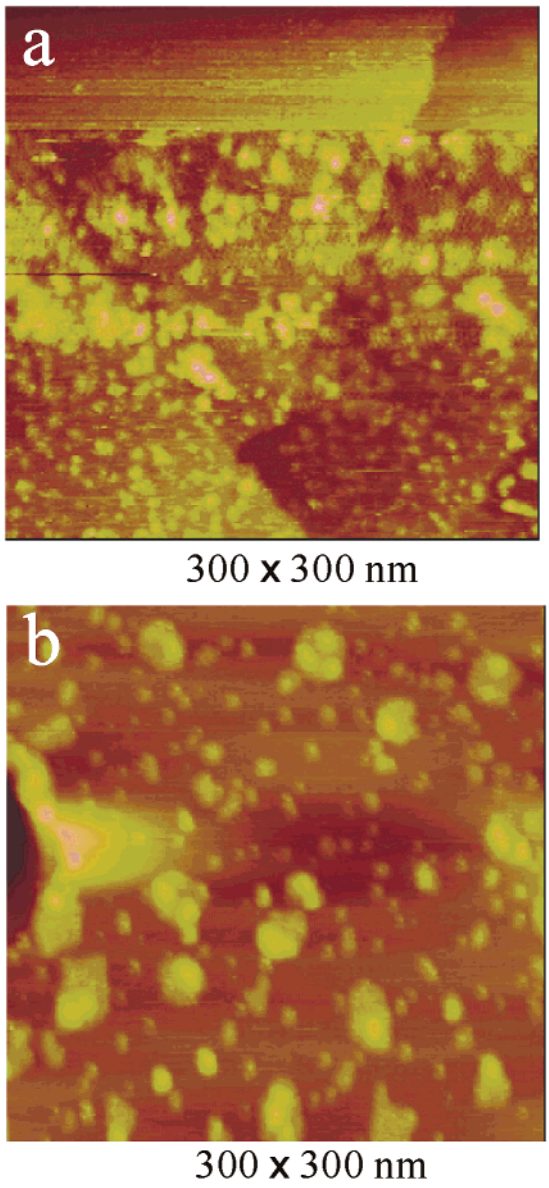

Figure 6. In situ STM images showing the instantaneous changes of surface morphology (a) and even distribution of Pt particles (b) on $PtBr_4^{2-}$-coated Au(111) after the potential was stepped from 0.9 to 0.4 V to induce reduction of Pt(II) to Pt(0). Image in (a) is a downward scan.

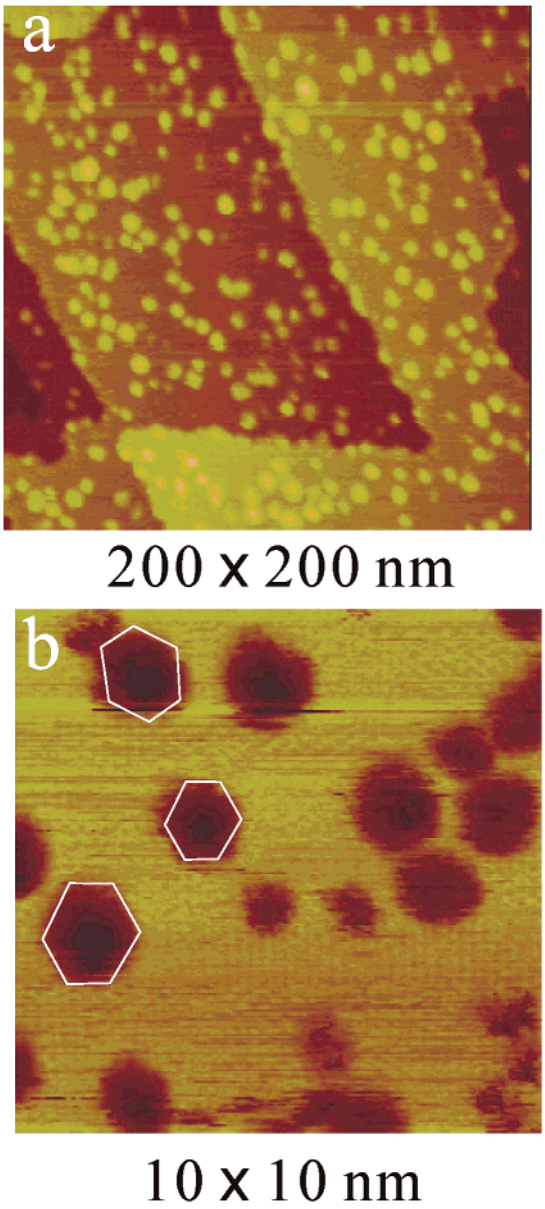

Figure 7. In situ STM images showing the even distribution of Pt particles (a) produced by electrochemical reduction of PtI_6^{2-} on Au-(111). In (b) a higher resolution STM scan, presented in an inverted mode, shows the hexagonal shapes of the Pt clusters appearing as depressions in the STM image. The potential of Au(111) is 0.3 V. I_{tip} and V_b are 2∼10 nA and 20∼100 mV, respectively.

the conditions used for the deposition, such as the overpotential and the concentration of Pt complexes, govern the outcome of Pt deposition.

The results obtained by using PtI_6^{2-} complex as the precursor to make Pt clusters were similar to those described above for $PtBr_4^{2-}$; i.e., randomly distributed clusters with diameters of a few nanometers were observed. Figure 7a shows a typical STM image of Au(111) at 0.25 V, where PtI_6^{2-} admolecules were fully reduced to Pt(0). Despite the presence of many steps and kinks in this area, Pt deposition took place without any preference toward these defects. Rather, domain boundaries within the molecular adlayers and pits on the terraces served as the nucleation sites for the deposition of Pt. To illustrate the shape of these Pt particles, a higher resolution STM scan presented in an "inverted" mode is shown in Figure 7b. The ordered lattice in the background is that of the Au(111) substrate, where the apparent depressions are actually the protruded Pt particles. These features suggest that the Pt clusters can be crystalline. Unfortunately, it is intrinsically difficult to achieve high-quality STM atomic resolution for a bumpy surface like this. In addition, the Pt clusters are probably atomically rough, which makes atomic resolution even more difficult to achieve. The size of the Pt particles varied between 1.0 and 6.0 nm, with a mean at 3.0. The height of the particles appeared to increase with the size, but it rarely exceeded three atomic layers. Typical clusters were 3.0 nm wide and 0.46 nm in height. The physical form of the Pt particles observed in this study resembles that reported on HOPG and on Au(111).[11,20] This clustering phenomenon is attributed to the high surface energy of Pt.[21] Finally, although the Au(111) − (1 × 1) surface is expected to reconstruct itself into (1 × 23) as the potential was stepped from 0.9 to 0.4 V in 0.1 M $HClO_4$,[28] in situ STM results indicate that the (1 × 1) surface remains unchanged. This seemingly contradictory result appears to be associated with the presence of Pt deposits on Au(111), inhibiting surface reconstruction.

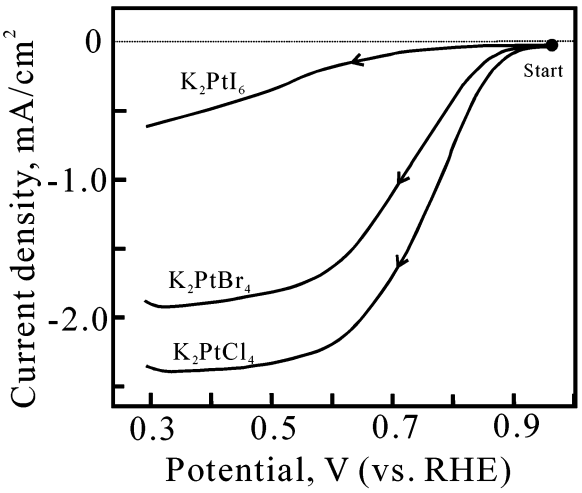

Figure 8. Rotating disk voltammograms at 50 mV/s for Pt-coated Au(111) electrodes immersed in oxygen-saturated 0.1 M $HClO_4$. Prior to these measurements, potentials were made negative enough to reduce these Pt complexes to Pt particles on Au(111). The rotation speed is 400 rpm.

To further confirm the presence of Pt particles on the Au(111) electrode, we conducted electrochemical measurements with a hanging-meniscus rotating Au disk electrode coated with Pt particles deposited from three Pt complexes, K_2PtCl_4, K_2PtBr_4, and K_2PtI_6, in oxygen-saturated 0.1 M $HClO_4$. The voltammograms are shown in Figure 8. For the cases of $PtBr_4^{2-}$ and $PtCl_4^{2-}$, the reduction of O_2 commences at 0.9 V, followed by a rapid increase of current up to 0.6 V, where the reaction becomes diffusion-controlled and the current levels off. Details of the reaction of oxygen reduction at particulate Pt electrodes will be reported elsewhere.[29] However, according to the previous studies, the reduction of oxygen molecules at Pt single crystalline electrodes proceeds mostly via the $4e^-$ reduction pathway to produce H_2O up to the potential where the adsorption of hydrogen atoms predominates.[30] In contrast, the reduction of oxygen molecules is inhibited if the Pt particles were prepared from PtI_6^{2-}. These results are explained by the strength of anion adsorption on Pt or Au electrodes. As evidenced by the STM results (Figure 5), iodine atoms, a known poison to the oxygen reduction reaction, are coadsorbed with the Pt complex. The strength of adsorption decreases in the order of I > Br > Cl so that the activity of Pt particles toward oxygen reduction is reversed.[25,26] On the other hand, because the amount of Pt particles produced from PtI_6^{2-} complex could be less than that from $PtCl_4^{2-}$ or $PtBr_4^{2-}$, the difference in current density might also be affected by Pt loadings.

Conclusion

Structures of adlayers of haloplatinate complexes on Au(111) prepared by a simple immersion method were examined by in situ STM under potential control. Both $PtCl_4^{2-}$ and $PtBr_4^{2-}$ adsorbed from solutions containing 50 μM of corresponding species form long-range ordered adlattices, identified as Au(111) $-$ $(\sqrt{7} \times \sqrt{7})R19.1°$, $\theta = 0.14$. Dosing Au(111) with dilute $PtBr_4^{2-}$ (5 μM) results in coadsorption of bromine atoms, which join in producing a mixed adlattice, characterized as $(2\sqrt{19} \times 2\sqrt{19})R23° - 7PtBr_4^{2-} + 6Br$. High-quality in situ STM imaging reveals pinwheel features for the square planar complexes of PtX_4^{2-} (X = Cl, Br, I), which are adsorbed in parallel configuration on Au(111). The monolayers of $PtCl_4^{2-}$, $PtBr_4^{2-}$, and PtI_6^{2-} molecules are reduced at 0.73, 0.45, and 0.32 V, respectively, to produce Pt particles distributed evenly on Au(111). Most Pt particles are 3.0 nm wide and 0.46 nm high. The frequently observed hexagonal shapes suggest that the Pt nanoparticles can be crystalline. These particulate Pt electrodes, except those prepared from PtI_6^{2-}, exhibit a catalytic activity toward oxygen reduction similar to single crystalline Pt electrodes. Iodine atoms adsorbed at Pt and Au surfaces, as well as the somewhat lower Pt loading produced from PtI_6^{2-}, account for the lower current density for the reduction of oxygen molecules.

Acknowledgment. This work was supported by the Core Research for Evolutional Science and Technology (CREST) − Japan Science and Technology Agency (JST), and by the Ministry of Education, Culture, Sport, Science and Technology, a Grant-in-Aid for the COE project, Giant Molecules and Complex Systems, 2003. S.L.Y. acknowledges the financial support from National Science Council, Taiwan (NSC 92-2113-M-008-009). The authors thank Dr. Y. Okinaka for his help in writing this manuscript.

References and Notes

(1) Murray, C. B.; Kagan, C. R.; Bawendi, M. G. *Annu. Rev. Mater. Sci.* **2000**, *30*, 545.
(2) Haruta, M.; Tsubota, S.; Kobayashi, T.; Kageyama, H.; Genet, M.; Delmon, B. *J. Catal.* **1993**, *144*, 175. (b) Valden, M.; Lai, X.; Goodman, D. W. *Science* **1998**, *261*, 1447.
(3) Templeton, A. C.; Wuelfing, W. P.; Murray, R. W. *Acc. Chem. Res.* **2000**, *33*, 27.
(4) Sawant, P.; Kovalev, J. T.; Efrima, S. *Langmuir* **2001**, *17*, 2913.
(5) Rodriguez, A.; Amiens, C.; Chaudret, B. *Chem. Mater.* **1996**, *8*, 1978.
(6) Joo, S. H.; Choi, S. J.; Oh, I.; Kwak, J.; Liu, Z.; Terasaki, O.; Ryoo, R. *Nature* **2001**, *412*, 169.
(7) Sasaki, M.; Osada, M.; Higashimoto, N.; Yamamoto, T.; Fukuoka, A.; Ichikawa, M. *J. Mol. Catal. A: Chemical* **1999**, 141, 223.
(8) Wang, Z. L.; Ahmad, T. S.; El-Sayed, M. A. *Surf. Sci.* **1997**, *380*, 302.
(9) Zhu, J.; Somorjai, G. A. *Nano Lett.* **2001**, *1*, 8.
(10) Friedrich, K. A.; Henglein, F.; Stimming, U.; Unkauf, W. *Electrochim. Acta* **2000**, *45*, 3283.
(11) Zoval, J. V.; Lee, J.; Gorer, S.; Penner, R. M. *J. Phys. Chem. B* **1998**, *102*, 1166.
(12) Waszczuk, P.; Wieckowski, A.; Zelenay, P.; Gottesfeld, S.; Coutanceau, C.; Leger, J.-M.; Lamy, C. *J. Electroanal. Chem.* **2001**, *511*, 55.
(13) Kokkinidis, G.; Stoychev, D.; Lazarov, V.; Papoutsis, A.; Milchev, A. *J. Electroanal. Chem.* **2001**, *511*, 20.
(14) Grzeszczuk, M.; Poks, P. *Electrochim. Acta* **2000**, *45*, 4171.
(15) Jiang, J.; Kucernak, A. *J. Electroanal. Chem.* **2002**, *520*, 64.
(16) Watanabe, M.; Sei, H.; Stonehart, P. *J. Electroanal. Chem.* **1989**, *261*, 375.
(17) Uosaki, K.; Ye, S.; Naohara, H.; Oda, Y.; Haba, T.; Kondo, T. *J. Phys. Chem. B* **1997**, *101*, 7566.
(18) Naohara, H.; Ye, S.; Uosaki, K. *J. Phys. Chem. B* **1998**, *102*, 4366.
(19) Kibler, L. A.; Kleinert, M.; Randler, R.; Kolb, D. M. *Surf. Sci.* **1999**, *443*, 19.
(20) Waibel, H. F.; Kleinert, M.; Kibler, L. A.; Kolb, D. M. *Electrochim. Acta*. **2002**, *47*, 1461.
(21) Bauer, E.; van der Merwe, J. H. *Phys. Rev. B* **1986**, *33*, 3657.
(22) Brankovic, B. R.; Wang, J. X.; Adzic, R. R. *Surf. Sci*. **2001**, *474*, L173.
(23) Clavilier, J.; Rodes, A.; El Achi, K.; Zamakhchari, M. A. *J. Chim. Phys.* **1991**, *88*, 1291.
(24) *Encyclopedia of Electrochemistry of the Elements*; Bard, A. J., Ed.; Marcel Dekker: New York, 1976; Vol. VI.
(25) Itaya,K. *Prog. Surf. Sci*. **1998**, *58*, 121.
(26) Yamada, T.; Batina, N.; Itaya, K. *J. Phys. Chem.* **1995**, *99*, 8817.
(27) *CRC Handbook for Chemistry and Physics*, 70th ed.; CRC Press: Boca Raton, 1990.
(28) Kolb, D. M. In *Structure of Electrified Interfaces*; Lipkowski, J., Ross, P. N., Eds.; VCH: New York, 1992.
(29) Hara, M.; Nagahara,Y.; Yoshimoto, S.; Inukai, J.; Yau, S.-L.; K. Itaya *J. Phys. Chem. B*, manuscript in preparation.
(30) Markovic, N. M.; Gaseiger, H. A.; Ross, P. N., Jr. *J. Phys. Chem*. **1995**, *99*, 3411.